Supplement of Biogeosciences, 20, 1829–1841, 2023
https://doi.org/10.5194/bg-20-1829-2023-supplement

Biogeosciences Open Access EGU

Supplement of

Carbon cycle extremes accelerate weakening of the land carbon sink in the late 21st century

Bharat Sharma et al.

Correspondence to: Bharat Sharma (bharat.sharma.neu@gmail.com)

S1 Calculation of temperature sensitivity of NBP

The sensitivity of NBP flux to surface air temperature is calculated using linear regression method (Piao et al., 2013),

$$NBP_{detrended} = b_0 + b_1 . TAS_{detrended} + \epsilon \quad (1)$$

where $NBP_{detrended}$ refers to the detrended monthly timeseries of NBP and TAS refers to the detrended monthly timeseries of surface air temperature. The regression coefficient b_1 represent the apparent sensitivity of NBP to TAS; b_0 is the fitted intercept; ϵ is the residue error in the linear regression. The sensitivities of tropical and high latitudinal regions, as shown in Figure 6, has been calculated for consequentive 10 years periods starting from 1850 to 2100. The detrended timeseries of NBP and TAS for every SREX region were calculated by calculating the difference of area weighted mean and 10 year moving average of respective variables. Positive temperature sensitivity to NBP signifies strengthening the impact of temperature on net biospheric carbon flux and vice versa.

Table S1. SREX Reference Regions

Abreviation	Region's Full Name
ALA	Alaska/N.W. Canada
AMZ	Amazon
CAM	Central America/Mexico
CAS	Central Asia
CEU	Central Europe
CGI	Canada/Greenland/Iceland
CNA	Central North America
EAF	East Africa
EAS	East Asia
ENA	East North America
MED	South Europe/Mediterranean
NAS	North Asia
NAU	North Australia
NEB	North-East Brazil
NEU	North Europe
SAF	Southern Africa
SAH	Sahara
SAS	South Asia
SAU	South Australia/New Zealand
SEA	Southeast Asia
SSA	Southeastern South America
TIB	Tibetan Plateau
WAF	West Africa
WAS	West Asia
WNA	West North America
WSA	West Coast South America

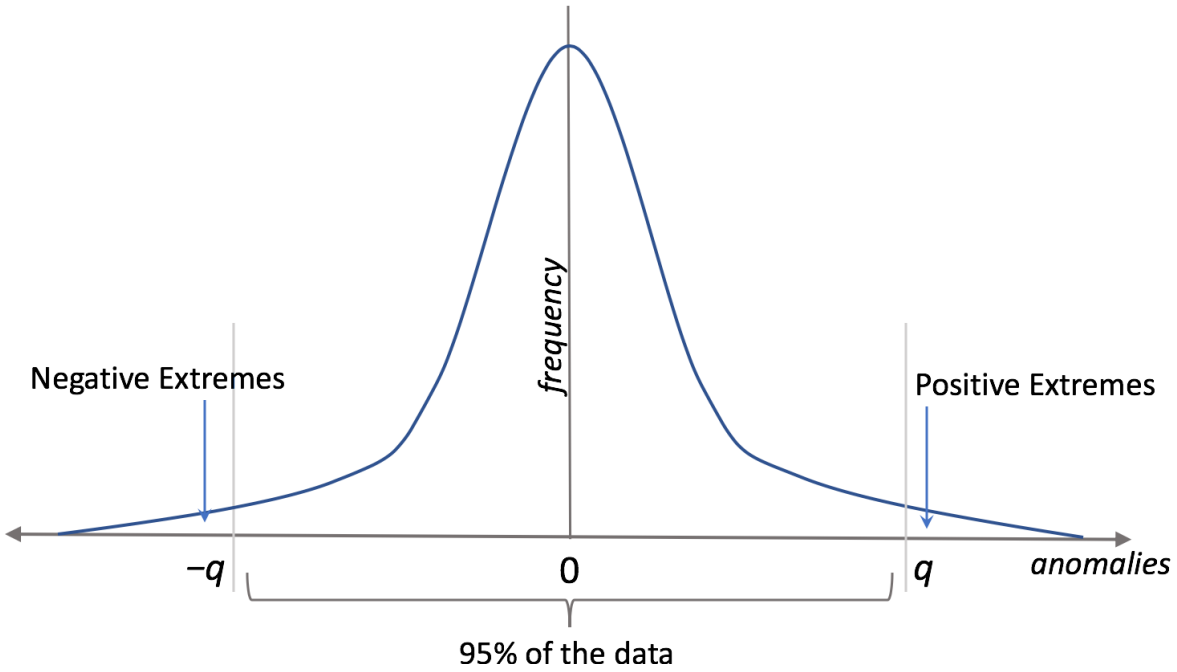

Figure S1. The schematic diagram representing the NBP extremes. The threshold q is set at 5^{th} percentile in this study, such that 95% of the NBP anomalies lie within $-q$ and q.

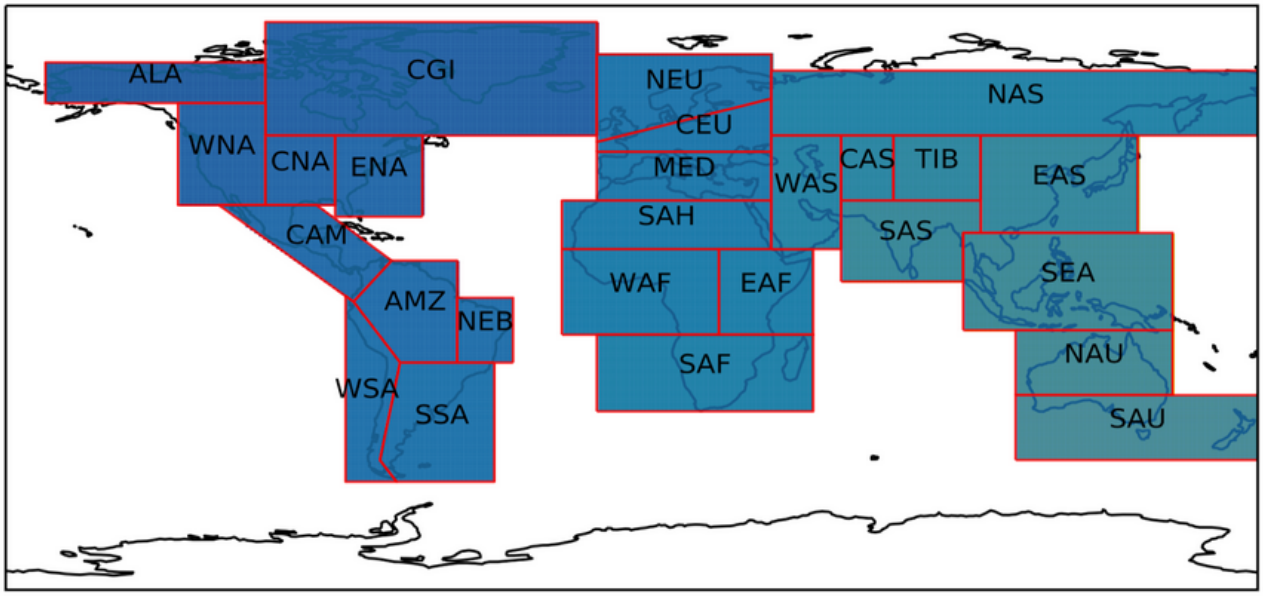

Figure S2. The spatial extent of SREX reference regions; abbreviations mentioned in the Table S1.

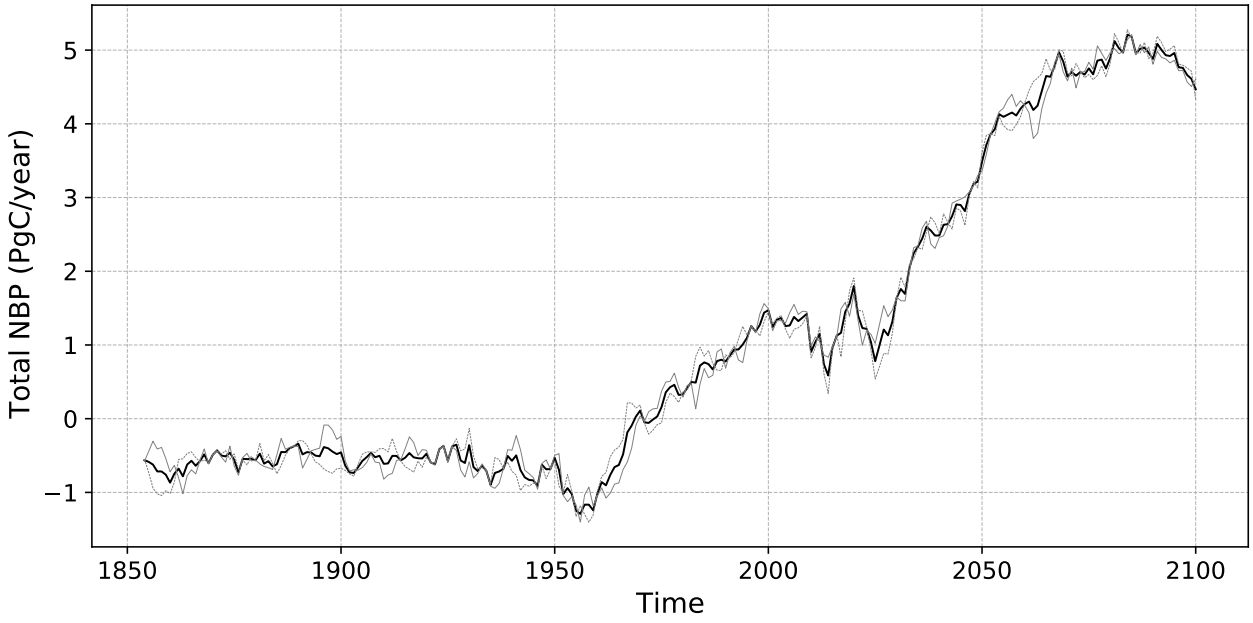

Figure S3. The timeseries of globally integrated 5 year rolling mean of NBP from 1850–2100 for CESM2 ensemble members is shown in gray dashed lines. The timeseries of globally integrated 5 year rolling mean of multi-ensemble mean is shown in black solid line.

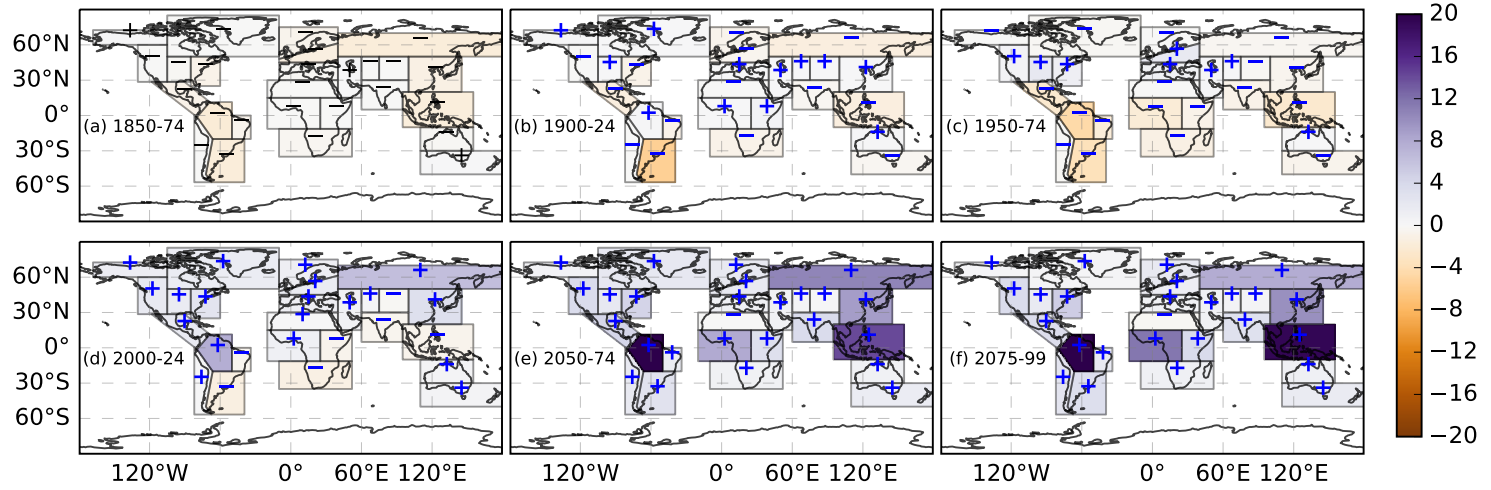

Figure S4. Total integrated NBP (PgC) for 25-year time windows for the period 1850–2100. Spatial distribution of integrated NBP (PgC) change over time: (a) 1850–74, (b) 1900–24, (c) 1950–74, (d) 2000-24, (e) 2050–74, and (f) 2075–99. Net increase in regional NBP or total carbon uptake is represented by purple color and '+' sign; net decrease is represented by orange color and '−' sign.

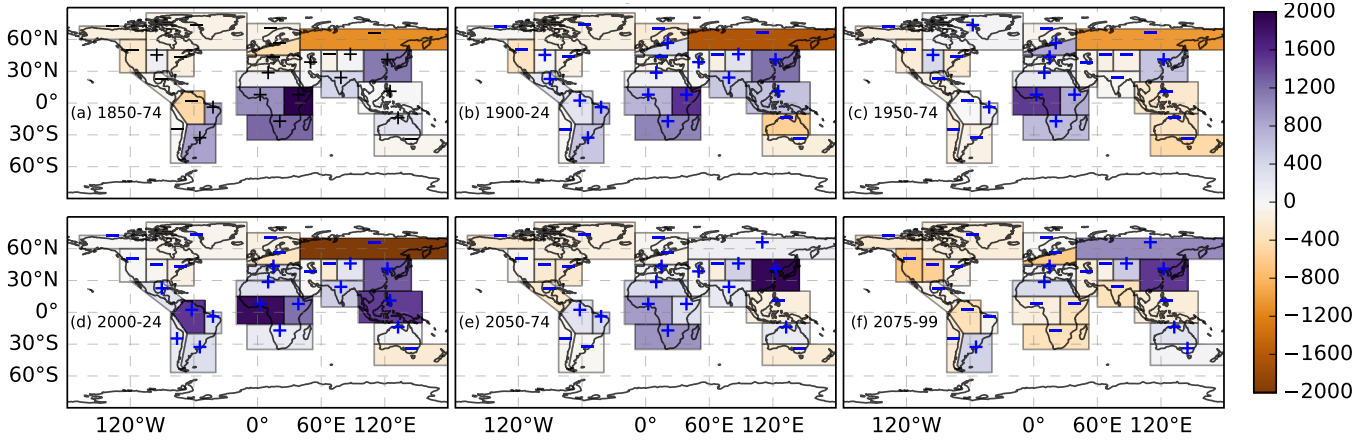

Figure S5. Frequency of positive *vs* negative NBP extreme events across SREX regions. Purple color ('+' sign) highlights the regions where frequency of positive NBP extremes events exceed negative NBP extremes; and brown color ('−' sign) identifies regions where frequency of negative NBP extreme events exceed positive NBP extremes. Towards the end of 21st century, most tropical regions are dominated by frequent negative NBP extremes.

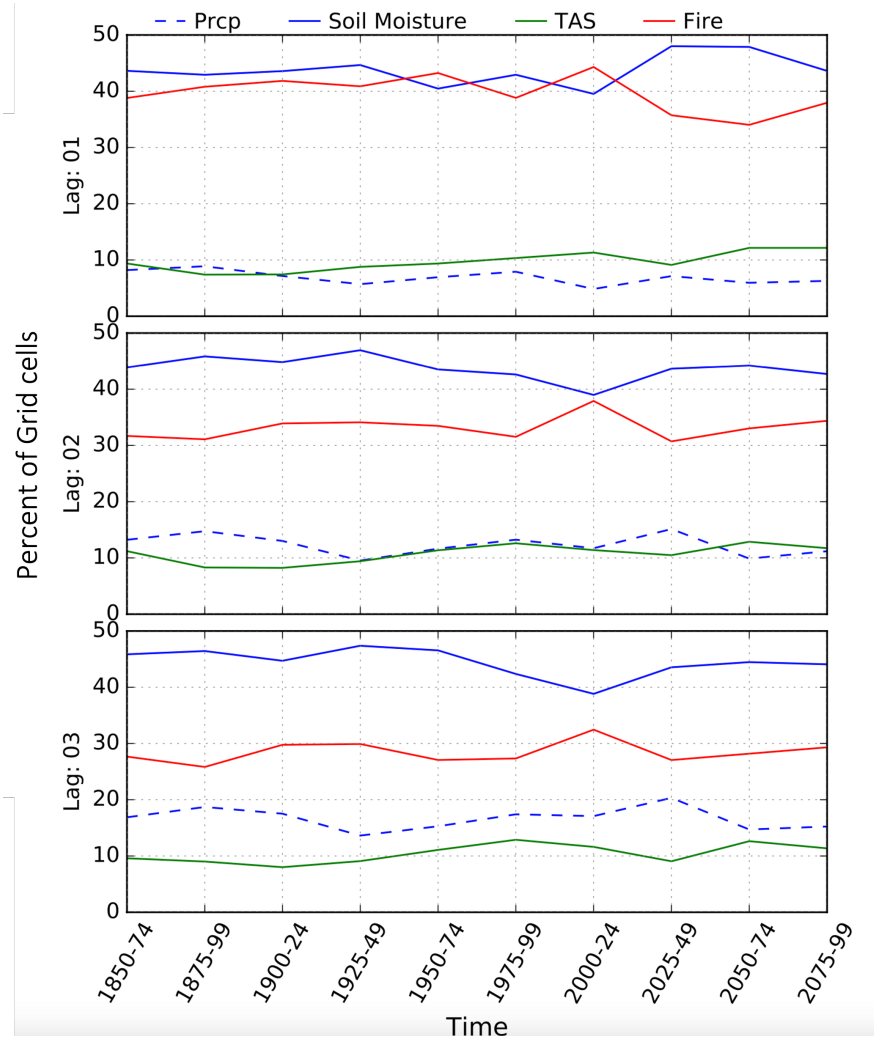

Figure S6. Percent distribution of number of grid cells with dominant climate drivers causing time continuous carbon cycle extremes from 1850 to 2100 for every 25-year period. The dominance of climate drivers is estimated by the absolute magnitude of correlation coefficient ($p < 0.05$) at lags of 1 (*top*), 2 (*middle*), and 3 (*bottom*) months.

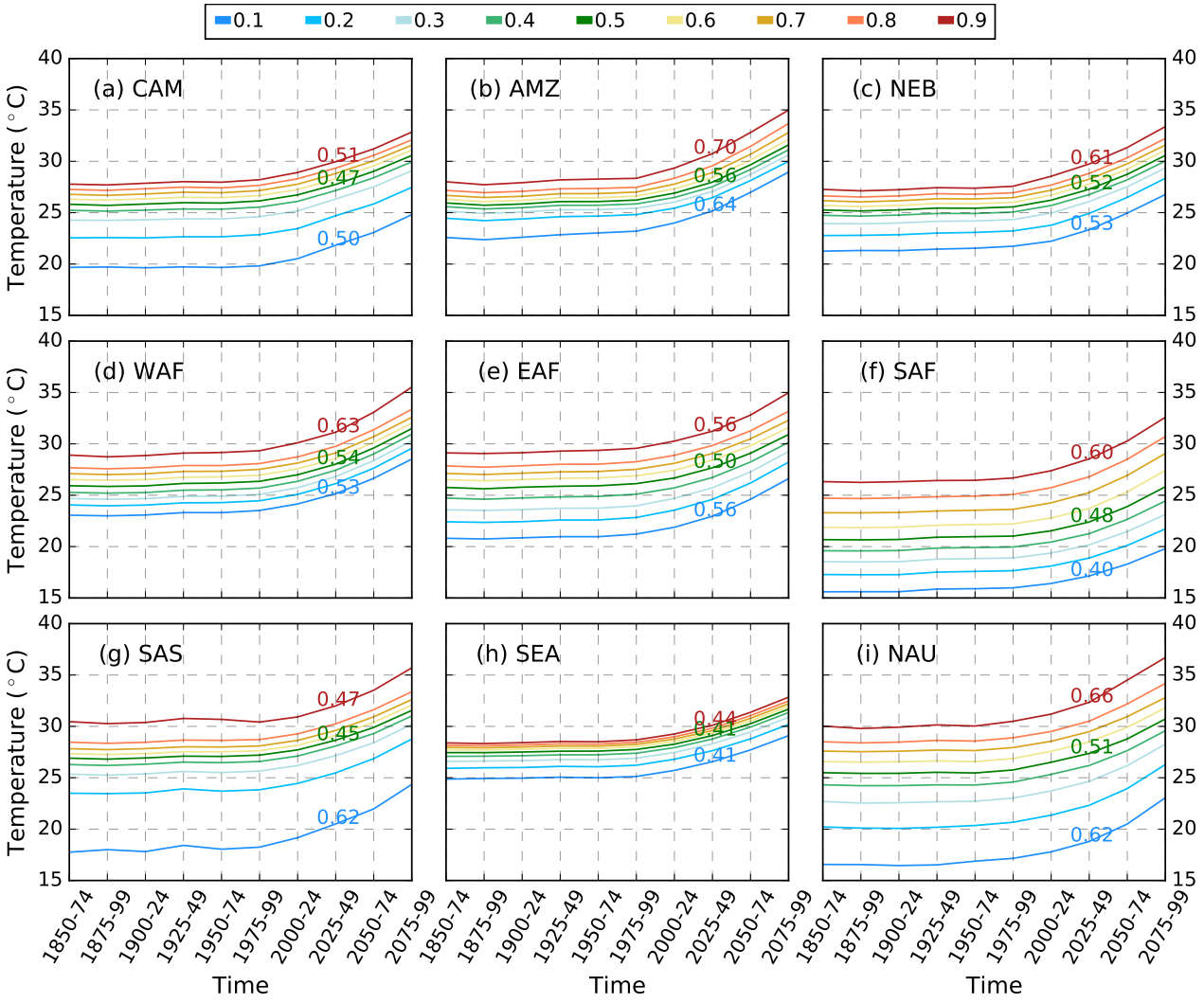

Figure S7. Change in area weighted average surface temperature (TAS) at various quantiles in the 9 SREX regions in tropics for 25-year windows from 1850–2100. The numbers shown in maroon, green, and blue in each subplot represent the rate of increase of temperature per decade (°C/decade) for 90^{th}, median, and 10^{th} quantile of temperatures, respectively.

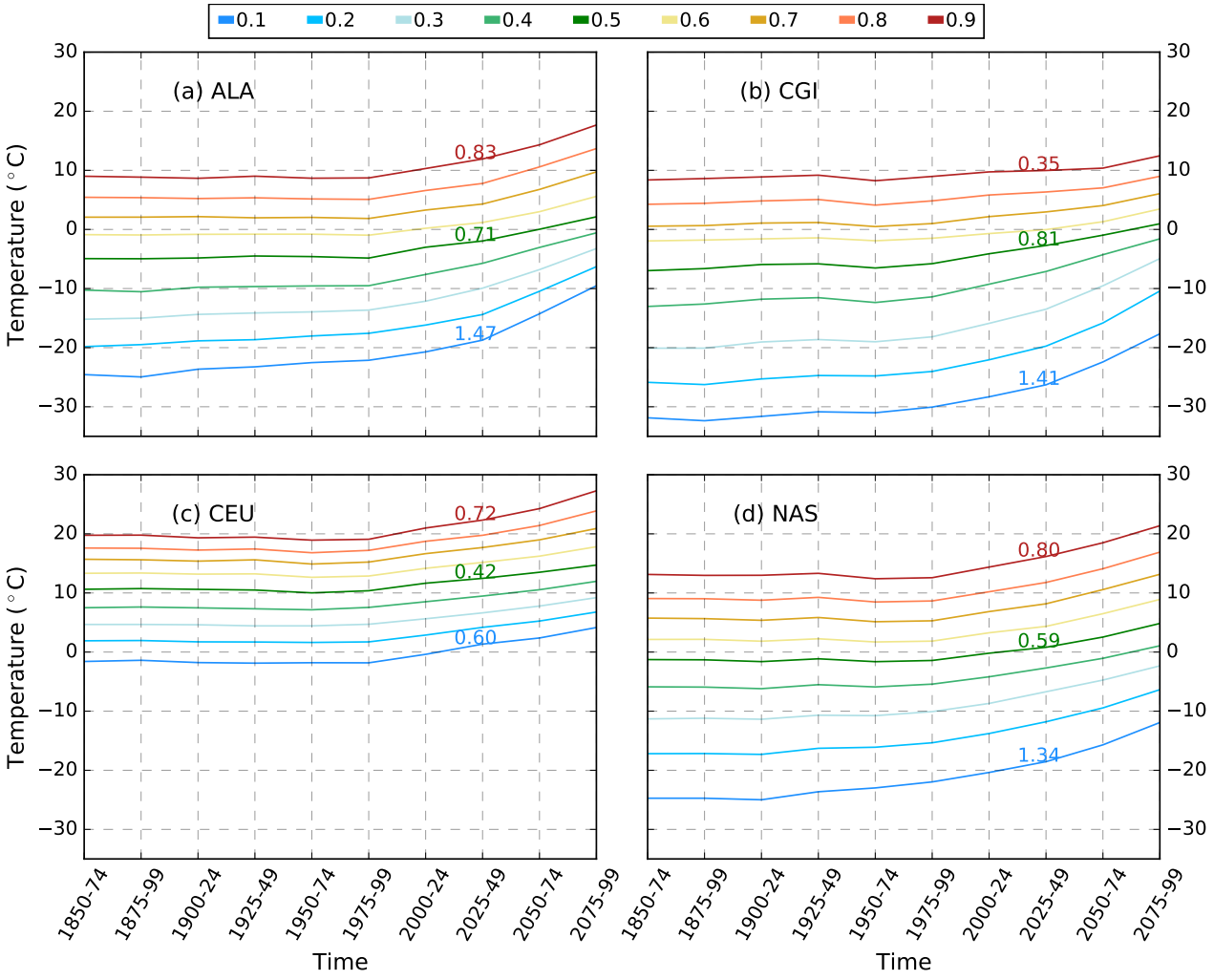

Figure S8. Change in area weighted average surface temperature (TAS) at various quantiles in the 9 SREX regions at high latitudes for 25-year windows from 1850–2100. The numbers shown in maroon, green, and blue in each subplot represent the rate of increase of temperature per decade (°C/decade) for 90^{th}, median, and 10^{th} quantile of temperatures, respectively.

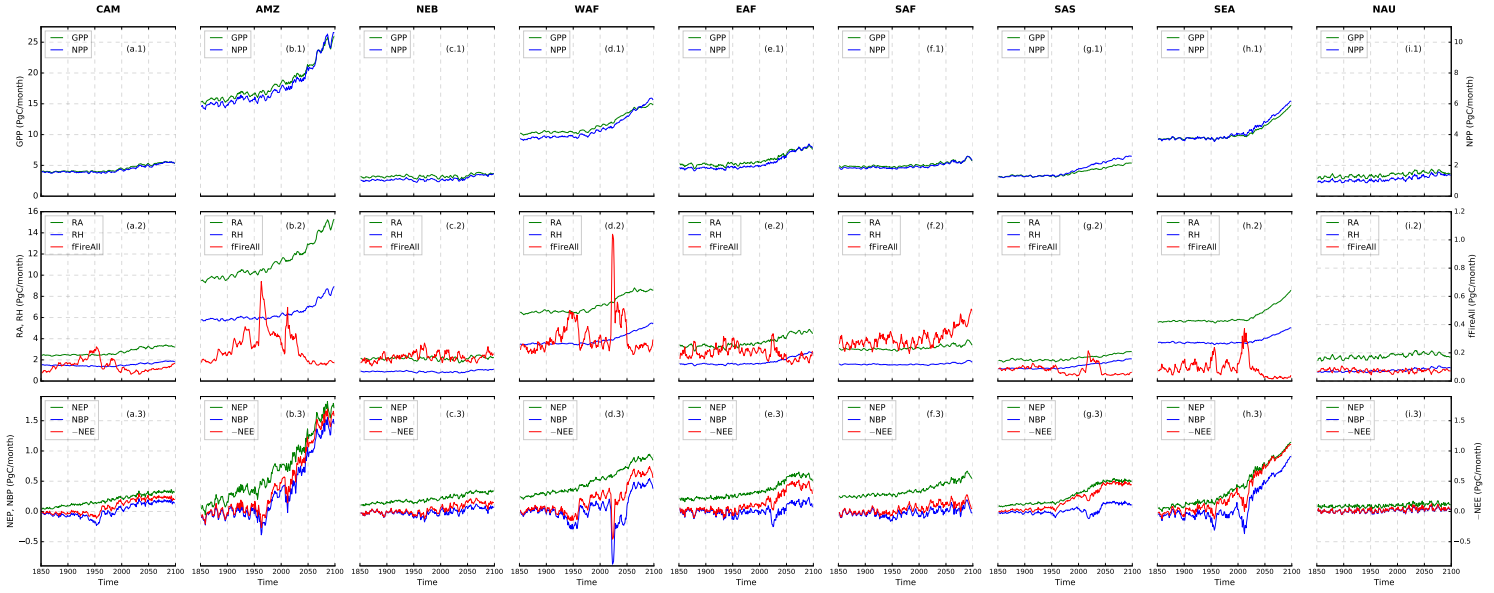

Figure S9. Timeseries of total carbon fluxes for the regions of (a) Central America/Mexico (CAM), (b) Amazon(AMZ), (c) North-East Brazil (NEB), (d) West Africa (WAF),(e) East Africa (EAF), (f) Southern Africa (SAF), (g) South Asia (SAS), (h) Southeast Asia (SEA), and (i) North Australia (NAU) . Row 1 for each region shows the time series of total GPP (left y-axis) and NPP (right y-axis). Row 2 shows RA and RH on left y-axis and fFireAll on right y-axis. Row 3 shows NEP, NBP on left y-axis and −NEE on right y-axis. NEP is calculated by subtracting RH from NPP. NEP is surface net downward mass flux of carbon dioxide expressed as carbon due to all land processes excluding anthropogenic land use change. −NEE has the consistent direction with the carbon flux such as NBP and NPP.

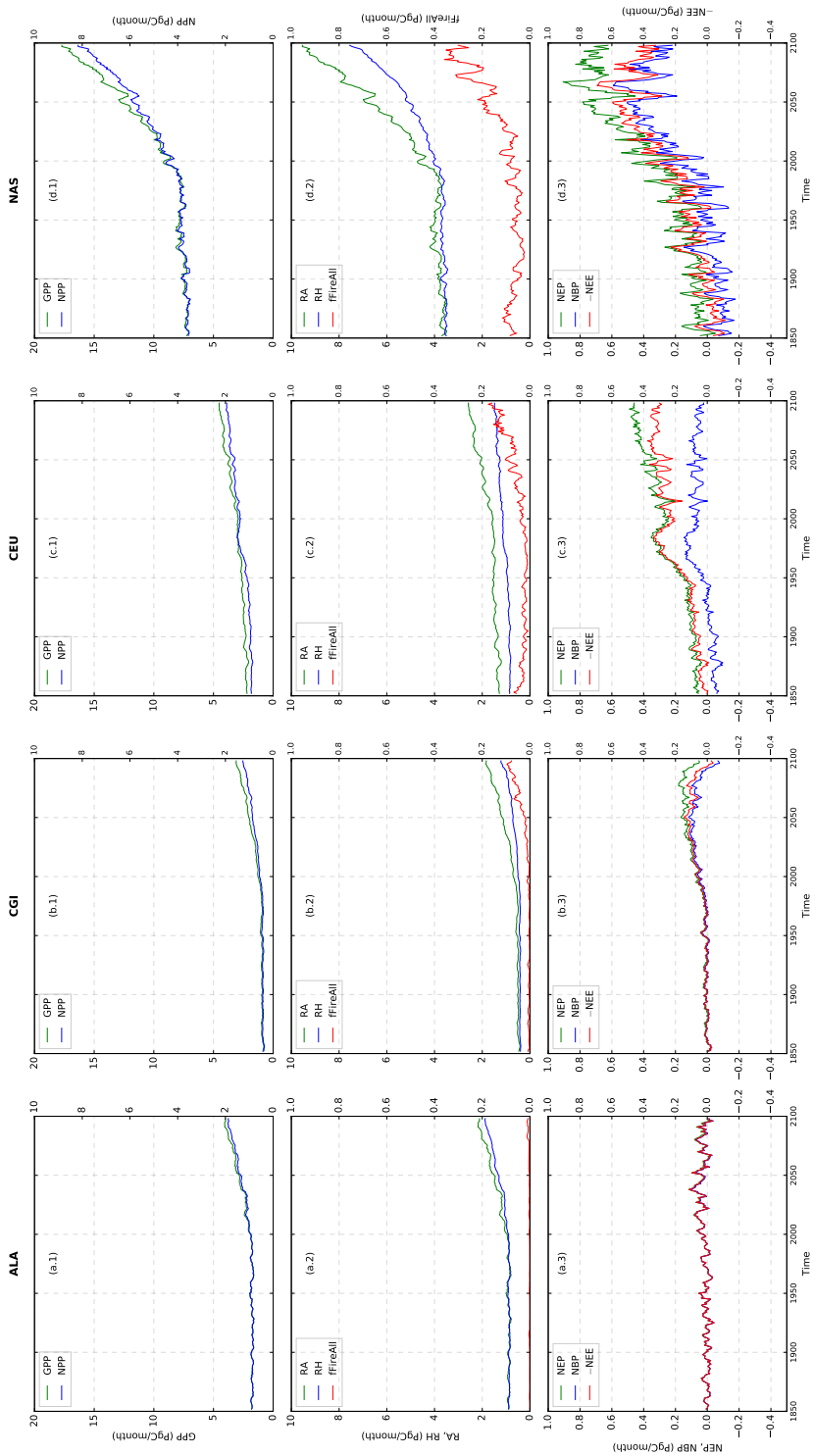

Figure S10. Timeseries of total carbon fluxes for the regions of (a) Alaska, (b) Canada, Greenland, and Iceland, (c) Central Europe, and (d) Northern Asia (NAS). Row 1 of every region shows the time series of total GPP (left y-axis) and NPP (right y-axis). Row 2 shows RA and RH on left y-axis and fFireAll on right y-axis. Row 3 shows NEP, NBP on left y-axis and −NEE on right y-axis. NEP is calculated by subtracting RH from NPP. NEP is surface net downward mass flux of carbon dioxide expressed as carbon due to all land processes excluding anthropogenic land use change. −NEE has the consistent direction with the carbon flux such as NBP and NPP.

References

Piao, S., Sitch, S., Ciais, P., Friedlingstein, P., Peylin, P., Wang, X., Ahlström, A., Anav, A., Canadell, J. G., Cong, N., Huntingford, C., Jung, M., Levis, S., Levy, P. E., Li, J., Lin, X., Lomas, M. R., Lu, M., Luo, Y., Ma, Y., Myneni, R. B., Poulter, B., Sun, Z., Wang, T., Viovy, N., Zaehle, S., and Zeng, N.: Evaluation of terrestrial carbon cycle models for their response to climate variability and to CO2 trends, Global Change Biology, 19, 2117–2132, https://doi.org/10.1111/gcb.12187, 2013.